

Lamin A/C Depletion Enhances DNA Damage-Induced Stalled Replication Fork Arrest

Mayank Singh,^{a,*} Clayton R. Hunt,^{a,e} Raj K. Pandita,^{b,e} Rakesh Kumar,^{a,e*} Chin-Rang Yang,^{c,*} Nobuo Horikoshi,^{a,e} Robert Bachoo,^d Sara Serag,^a Michael D. Story,^a Jerry W. Shay,^b Simon N. Powell,^{e*} Arun Gupta,^{a,e} Jessie Jeffery,^f Shruti Pandita,^e Benjamin P. C. Chen,^a Dorothee Deckbar,^g Markus Löbrich,^g Qin Yang,^e Kum Kum Khanna,^f Howard J. Worman,^h Tej K. Pandita^{a,e}

Department of Radiation Oncology,^a Department of Cell Biology,^b Simmons Cancer Center,^c and Department of Neuro-oncology,^d UT Southwestern Medical Center, Dallas, Texas, USA; Department of Radiation Oncology, Washington University School of Medicine, St. Louis, Missouri, USA^e; Signal Transduction Laboratory, Queensland Institute of Medical Research, Brisbane, Queensland, Australia^f; Darmstadt University of Technology, Darmstadt, Germany^g; Department of Medicine and Department of Pathology and Cell Biology, College of Physicians and Surgeons, Columbia University, New York, New York, USA^h

The human *LMNA* gene encodes the essential nuclear envelope proteins lamin A and C (lamin A/C). Mutations in *LMNA* result in altered nuclear morphology, but how this impacts the mechanisms that maintain genomic stability is unclear. Here, we report that lamin A/C-deficient cells have a normal response to ionizing radiation but are sensitive to agents that cause interstrand cross-links (ICLs) or replication stress. In response to treatment with ICL agents (cisplatin, camptothecin, and mitomycin), lamin A/C-deficient cells displayed normal γ -H2AX focus formation but a higher frequency of cells with delayed γ -H2AX removal, decreased recruitment of the FANCD2 repair factor, and a higher frequency of chromosome aberrations. Similarly, following hydroxyurea-induced replication stress, lamin A/C-deficient cells had an increased frequency of cells with delayed disappearance of γ -H2AX foci and defective repair factor recruitment (Mre11, CtIP, Rad51, RPA, and FANCD2). Replicative stress also resulted in a higher frequency of chromosomal aberrations as well as defective replication restart. Taken together, the data can be interpreted to suggest that lamin A/C has a role in the restart of stalled replication forks, a prerequisite for initiation of DNA damage repair by the homologous recombination pathway, which is intact in lamin A/C-deficient cells. We propose that lamin A/C is required for maintaining genomic stability following replication fork stalling, induced by either ICL damage or replicative stress, in order to facilitate fork regression prior to DNA damage repair.

Lamins are intermediate filament proteins that form a protein meshwork lining the inner nuclear membrane, where they contribute to maintaining the shape and mechanical stability of the nucleus (1). Lamin proteins interact with histone H2A (2, 3) and also form nucleoplasmic foci that perform dynamic organizational roles in the nucleus (4, 5). Human lamins A and C (lamin A/C) are generated from a single *LMNA* gene (*Lmna* in mice) by alternative splicing, and mutations that disrupt splicing are the basis for a variety of degenerative disorders, including premature aging syndromes and cancer. Mutations in the *LMNA* gene have also been linked to chromatin modifications that, when defective, are associated with altered DNA transcription, replication, and repair. About 200 disease-associated *LMNA* mutations have been identified (6), and the resulting laminopathies all are characterized by chromosomal aberrations (7, 8). Although lamins are implicated in chromatin organization, DNA replication, RNA polymerase II-dependent gene expression, and DNA damage response (DDR) (8–11), *Lmna* deletion in mice is not lethal (12, 13). However, cells from *Lmna*^{−/−} mice do display loss of chromatin integrity with deformation or blebbing of the lamina and nuclear envelope (13). Chromatin changes related to loss of structural shape, in conjunction with transcription regulatory changes (12, 14, 15), can also alter the DDR, resulting in DNA damage accumulation (16). While chromatin changes have been linked with altered gene expression, altered expression of DDR-related genes due to lamin A/C deficiency have not yet been identified. We compared the gene expression profile between cells with and without *Lmna* and report here that loss of lamin A/C results in decreased cyclin D1 levels. In an examination of clonogenic survival and DNA damage response/repair, we found that cells deficient in lamin A/C have

decreased survival, defective DNA damage response, and decreased restart of stalled replication forks after exposure to agents that cause interstrand cross-links (ICLs), DNA adducts, and replication stress.

MATERIALS AND METHODS

Colony-forming assay and chromosomal aberration analysis. *Lmna*^{+/+}, *Lmna*^{−/−}, 293, MCF7, and GM5849 cells were maintained and transfected with plasmids as described previously (17, 18). A cDNA fragment encoding wild-type lamin A was cloned into the mammalian expression vector pcDNA3.1 (Invitrogen, Carlsbad, CA) as described previously (17, 19). Small interfering RNAs (siRNAs) for human *LMNA*, cyclin D1, RAD51, ORCA1, polymerase η (Pol η), and control luciferase (Luc) were obtained from Dharmacon Research (Lafayette, CO). RNA interference (RNAi) treatment of cell lines was performed as described previously (17, 19, 20). Cells were used 72 h after transfection for all experimental purposes. Colony-forming assays and analysis of metaphase spreads to mea-

Received 11 December 2012 Accepted 3 January 2013

Published ahead of print 14 January 2013

Address correspondence to Tej K. Pandita, tej.pandita@utsouthwestern.edu.

M.S., C.R.H., R.K.P., R.K., and C.-R.Y. contributed equally.

* Present address: Mayank Singh, AllMS, Rishikesh, India; Rakesh Kumar, Shri Mata Vaishno Devi University Campus, Katra, Jammu, India; Simon N. Powell, Department of Radiation Oncology, Memorial Sloan-Kettering Cancer Center, New York, New York, USA; Chin-Rang Yang, National Heart Lung and Blood Institute, NIH, Bethesda, Maryland, USA.

Copyright © 2013, American Society for Microbiology. All Rights Reserved.

doi:10.1128/MCB.01676-12

sure chromosomal aberrations were carried out as described previously (20).

Microirradiation. *Lmna*^{+/+} and *Lmna*^{-/-} cells expressing yellow fluorescent protein (YFP)-labeled polymerase η were grown on coverslips. Microirradiation and quantification of polymerase η signal at different time points postirradiation was done as described previously (18).

Cell cycle analysis. Murine embryonic fibroblasts (MEFs) were synchronized by culturing in Dulbecco's modified Eagle medium (DMEM) containing 0.1% fetal calf serum (FCS) for 72 h and then stimulated with DMEM supplemented with 10% FCS at various time points. After serum stimulation, cells were harvested by trypsinization and processed for fluorescence-activated cell sorter (FACS) analysis by a previously described procedure (21, 22). To determine the frequency of S-phase cells after nocodazole treatment, *Lmna*^{+/+} and *Lmna*^{-/-} cells were treated for 20 h with nocodazole to arrest them in G₂/M, and after release cells were harvested at the indicated time points, stained with propidium iodide (PI), and subjected to FACS analysis to determine percentage of cells entering G₁ phase.

Immunofluorescence microscopy. Cell culture in chamber slides, fixation, and immunostaining were done as previously described (23–25). For depletion of lamin A/C, 293 cells were transfected with the specific siRNA and allowed to grow for 48 h before treatment with the indicated DNA-damaging agent or mock treatment. Cells then were treated with an extraction buffer for 5 min before fixation in 4% paraformaldehyde (PFA). A standard procedure for capturing fluorescent images of foci was followed (26). Sections through nuclei were captured, and the images were obtained by projection of the individual sections as recently described (27). The results shown are from three to four independent experiments.

Expression profiling. A previously described method was used for microarray analysis of gene expression (28). Total RNA was isolated from cells using the RNeasy kit (Qiagen), and gene expression analyses were performed using the Illumina mouse gene expression array (MouseWG-6 v2). The array images were processed using Illumina Genome Studio per the manufacturer's instructions, and the intensity values were background subtracted and quantile normalized. The differential gene expression was detected by fold change cutoff (≥ 2 or ≤ -2), and the gene list was uploaded to the ingenuity pathway analysis (IPA) program for cellular function enrichment and biological network analyses.

DNA replication restart assay. Exponentially growing cells were pulsed with 50 mM 5-iododeoxyuridine (IdU) for 20 min, washed three times with phosphate-buffered saline (PBS), treated with 2 mM hydroxyurea (HU) for the indicated intervals, washed three times with PBS, incubated in fresh medium containing with 50 mM 5-chlorodeoxyuridine (CldU) for 20 min, and then washed three times in PBS. DNA fiber spreads were made by a modified procedure described previously (29). Briefly, cells labeled with IdU and CldU were mixed with unlabeled cells in a ratio of 1:10, and 2- μ l cell suspensions were dropped onto a glass slide and then mixed with a 20- μ l hypotonic lysis solution (10 mM Tris-HCl, pH 7.4, 2.5 mM MgCl₂, 1 mM phenylmethylsulfonyl fluoride [PMSF], and 0.5% Nonidet P-40) for 8 min. Air-dried slides were fixed, washed with 1 \times PBS, blocked with 5% bovine serum albumin (BSA) for 15 min, and incubated with primary antibodies against IdU and CldU (rat monoclonal antibody [MAb] anti-IdU [1:150 dilution; Abcam] and mouse MAb anti-CldU [1:150 dilution; BD]) and secondary antibodies (anti-rat Alexa Fluor 488-conjugated [1:150 dilution] and anti-mouse Alexa Fluor 568-conjugated [1:200 dilution] antibodies) for 1 h each. Slides were washed with 1 \times PBS with 0.1% Triton X-100 and mounted with Vectashield mounting medium without 4',6-diamidino-2-phenylindole (DAPI). Image J software was used to analyze the DNA fibers.

Determination of collapsed replication fork. Mouse embryonic fibroblasts were labeled with 1 μ M 5-ethynyl-2'-deoxyuridine (EdU) for 30 min to stain S-phase cells, washed twice with 1 \times PBS, incubated in medium with 0.1 mM HU for 12 h, washed again with 1 \times PBS to remove HU, and incubated in fresh medium for 8 h after HU treatment. Cells were

stained for γ -H2AX and EdU, and EdU-positive G₂-phase cells (determined by their DAPI intensity) were evaluated. First, we scored only large γ -H2AX foci, which only arise after long HU treatment times and thus are supposed to represent collapsed replication forks (30). Second, we scored the percentage of EdU-positive cells, which migrated into G₁ during the 8-h time period after HU treatment. We found delayed progression into G₁ phase in *Lmna*^{-/-} cells. That is, despite the lower focus numbers, the *Lmna*^{-/-} cells did not readily progress into G₁, again consistent with the model that the lamin A/C-deficient cell is arrested in S phase because fork collapse is impaired.

MOF retention in *Lmna*^{+/+} and *Lmna*^{-/-} cells. Cells growing in exponential phase were irradiated and fixed with 4% formaldehyde at different times postirradiation, and total DNA was coimmunoprecipitated with MOF antibody after *in vivo* cross-linking by using the standard procedure described previously (31, 32). Immunoprecipitated DNA was purified by the phenol-chloroform procedure (33), DNA was quantified with a NanoDrop 2000 spectrometer (Thermo Scientific), and the amount of DNA retained by MOF is presented in arbitrary relative units of retention (MOF retention).

Telomeric circle detection and strand-specific FISH. Genomic DNA from exponentially growing cells was isolated, digested by standard protocols (31, 32), and fractionated on a 0.7% agarose gel containing 0.1 μ g/ml ethidium bromide in 1 \times Tris-acetate-EDTA at ~ 2 V/cm overnight. Neutral-neutral two-dimensional (2D) gel electrophoresis was performed according to the established protocols (34), with modifications as described previously (35). Strand-specific chromosome orientation fluorescent *in situ* hybridization (CO-FISH) was performed by the described procedure (26, 36).

RESULTS

Effect of lamin A/C depletion on gene expression. To elucidate the relationship between lamin A/C and genomic stability, a lamin A/C functional interaction network (Fig. 1A) based on the literature was first generated from IPA. Relative mRNA expression data were obtained by a microarray analysis of *Lmna*^{-/-} versus *Lmna*^{+/+} mouse embryonic fibroblast (MEF) RNA (Fig. 1B and C), and the up- and downregulated genes were overlaid on the IPA network (Fig. 1A). Lamin A/C clearly impacts multiple cellular functions (major altered functions are shown in Fig. 1A) and DNA damage repair, and the expression levels of several known DNA damage repair genes are also affected by lamin A/C (specific functions of interest are shown in Fig. 1C). The complete microarray data are available at <http://www.ncbi.nlm.nih.gov/geo/query/acc.cgi?acc=GSE38777>. We have summarized the top five genes that are up- or downregulated in *Lmna*^{-/-} cells compared to *Lmna*^{+/+} cells (Fig. 1C) in the following categories.

Cancer-related genes. Upregulated cancer-related genes are those for prostaglandin I₂ (prostaglandin synthase [PTGIS]), keratin 14 (KRT14), uroplakin 3B (UPK3B), keratin 8 (KRT8), and basonuclin 1 (BNC1). Downregulated genes are the genes for interferon-induced protein with tetratricopeptide repeats 3 (IFIT3), collagen type VI alpha 3 (COL6A3), alpha interferon-inducible protein 27-like 2 (IFI27L2), aquaporin 1 (Colton blood group) (AQP1), and fibroblast growth factor 7 (FGF7).

Proliferation and growth genes. Upregulated proliferation and growth genes are the transferrin (TF), KRT8, basonuclin 1 (BNC1), homeobox B7 (HOXB7), and tripartite motif-containing 25 (TRIM25) genes. Downregulated genes are those for cytochrome P450 family 7 subfamily B polypeptide 1 (CYP7B1), COL6A3, dickkopf homolog 3 (*Xenopus laevis*) (DKK3) FGF7, and lamin A/C (LMNA).

Cell cycle-related genes. Upregulated cell cycle-related genes

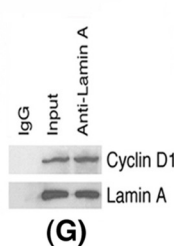
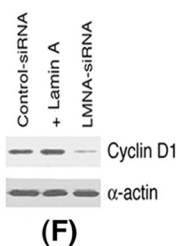
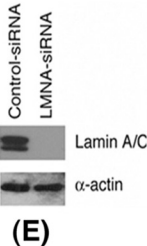
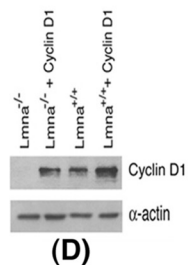
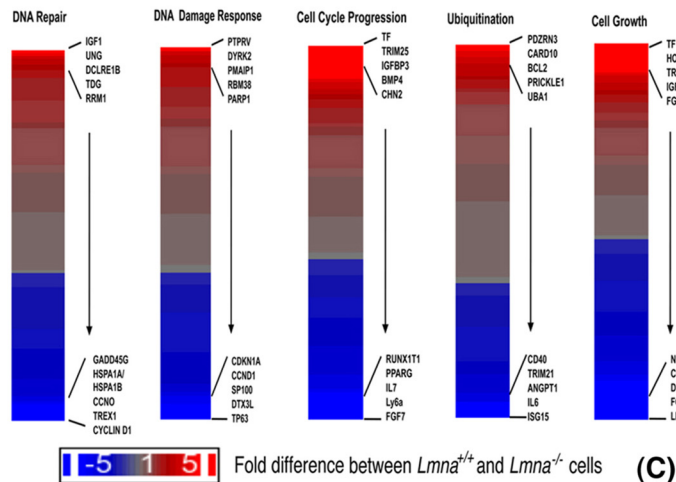
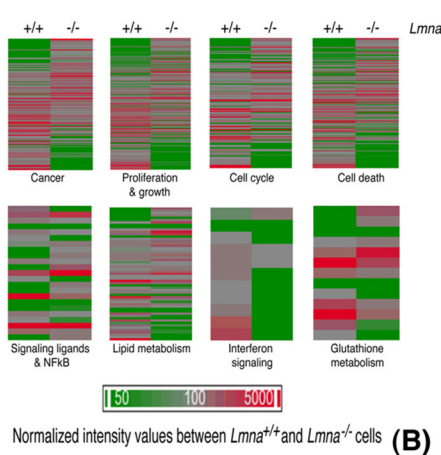
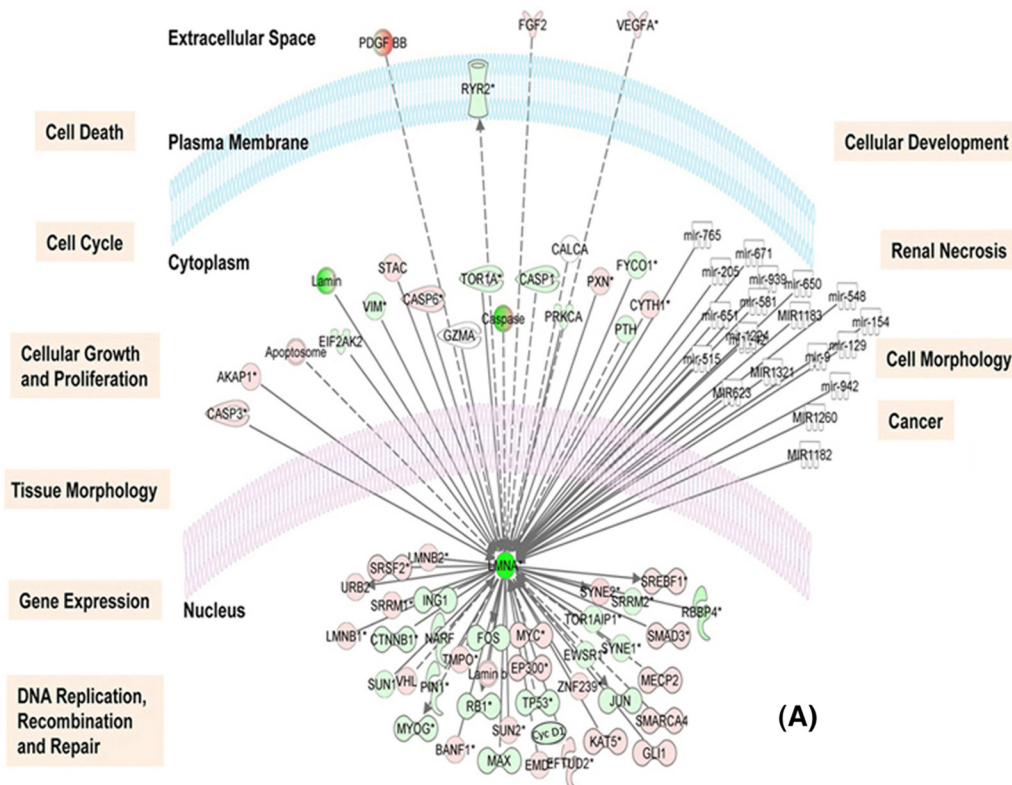


FIG 1 Functions of lamin A/C. (A) Ingenuity pathway analysis of lamin A/C based on mRNA microarray expression data from comparisons of mRNA from *Lmna*^{+/+} to that of *Lmna*^{-/-} cells. Pink indicates upregulated and green downregulated genes. The top 12 relevant biological functions and disease associations from the analysis are shown on both sides of the figure. (B) Comparison of mRNA expression status between *Lmna*^{+/+} and *Lmna*^{-/-} cells. The expression is organized into eight major groups involved in cellular metabolism. The eight major groups are cancer, proliferation and growth, cell cycle, cell death, signaling ligands and NF- κ B, lipid metabolism, interferon signaling, and glutathione metabolism. (C) mRNA expression is organized from highest to lowest in *Lmna*^{-/-} cells compared to *Lmna*^{+/+} cells. Details of the expression levels are available at <http://www.ncbi.nlm.nih.gov/geo/query/acc.cgi?acc=GSE38777>. (D) Western blot showing cyclin D1 protein levels in *Lmna*^{+/+} and *Lmna*^{-/-} cells. (E) Western blot showing lamin A/C knockdown by LMNA-specific siRNA. (F) Western blot showing decreased cyclin D1 levels in 293 cells treated with lamin A/C-specific siRNA. (G) Coimmunoprecipitation of endogenous lamin A/C and cyclin D1 with anti-lamin A/C antibody detected by immunoblotting.

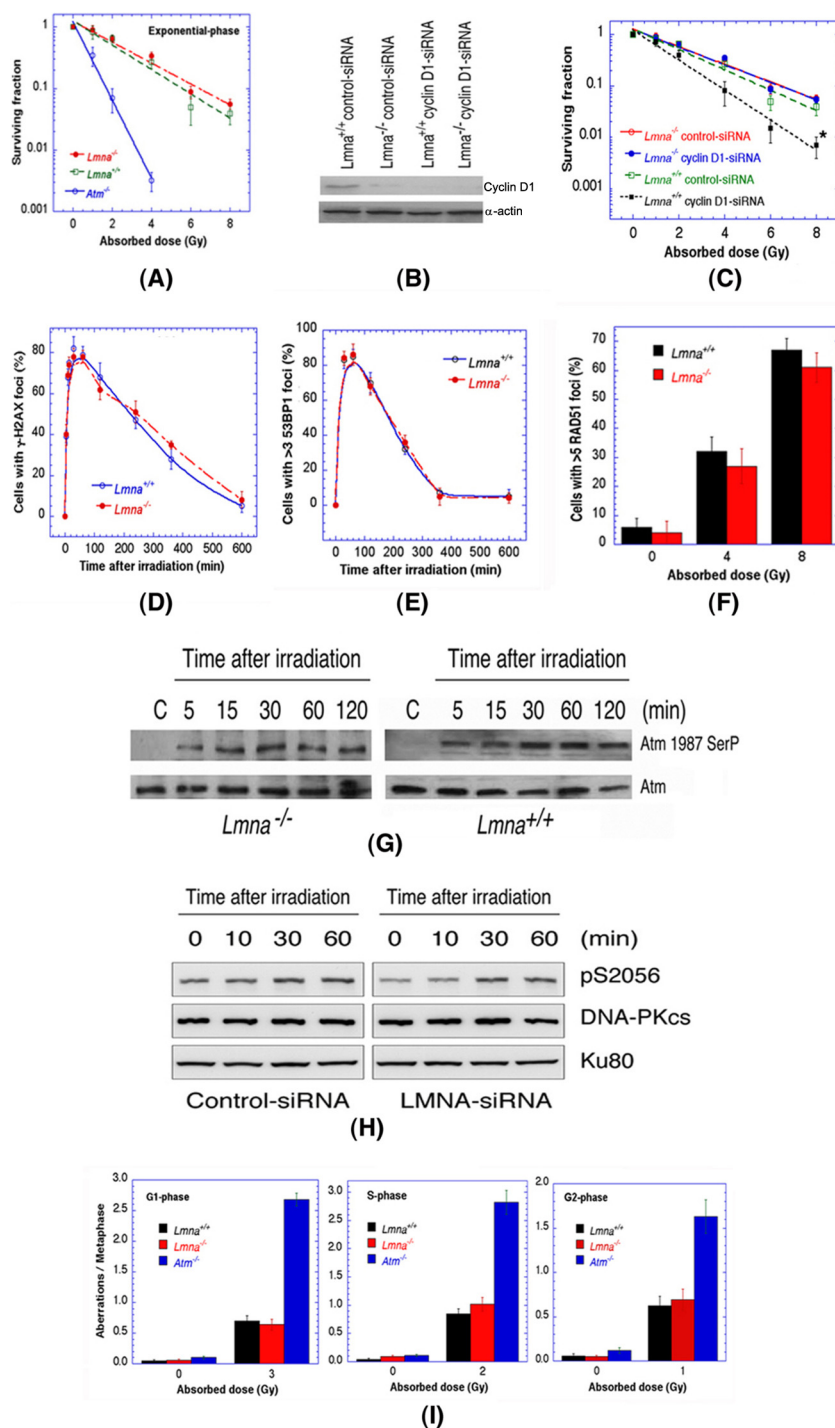


FIG 2 Ionizing radiation response in cells with and without lamin A/C. (A) Clonogenic survival of *Lmna*^{+/+} and *Lmna*^{-/-} mouse cells after exposure to increasing radiation doses. (B) Western blot showing depletion of cyclin D1 by specific siRNA in *Lmna*^{-/-} and *Lmna*^{+/+} cells. (C) Clonogenic survival of cells with and without cyclin D1 knockdown after exposure to graded doses of IR. (D) Exponentially growing cells were irradiated with 2 Gy, and the appearance/disappearance of γ -H2AX foci was determined by immunostaining. (E) *Lmna*^{+/+} and *Lmna*^{-/-} cells were irradiated with 6 Gy, and 53BP1 focus formation was quantified by immunostaining at different time points postirradiation. (F) Exponential-phase *Lmna*^{+/+} and *Lmna*^{-/-} cells were irradiated with different IR doses, and RAD51 focus formation was quantified 4 and 8 h postirradiation. (G) Ionizing radiation-induced phosphorylation of ATM Ser1981, detected by immunoblotting, in exponentially growing *Lmna*^{+/+} and *Lmna*^{-/-} cells after irradiation with 5 Gy. (H) Ionizing radiation-induced phosphorylation of DNA-PK catalytic subunit (DNA-PKcs) in 293 cells with and without siRNA depletion of lamin A/C detected by DNA-PKcs and phospho-Ser2056 immunoblotting. Cells were irradiated with 10 Gy and collected at different time points postirradiation for analysis. (I) Chromosomal aberrations in *Lmna*^{+/+} and *Lmna*^{-/-} cells after IR exposure. For analysis of G₁-phase aberrations, cells were irradiated (3 Gy), incubated for 12 h, and then treated for 3 h with colcemid before collecting metaphases for scoring. Categories of asymmetric chromosome aberrations scored included dicentric, centric rings, interstitial deletions-acentric rings, and terminal deletions. For S-phase-specific aberrations, cells were irradiated with 2 Gy and incubated for 6 h, and metaphases were harvested after 3 h of colcemid treatment. For G₂-type chromosome aberrations, exponential-phase cells were irradiated (1 Gy) and incubated for 1 h, followed by 3 h of colcemid treatment to collect metaphases.

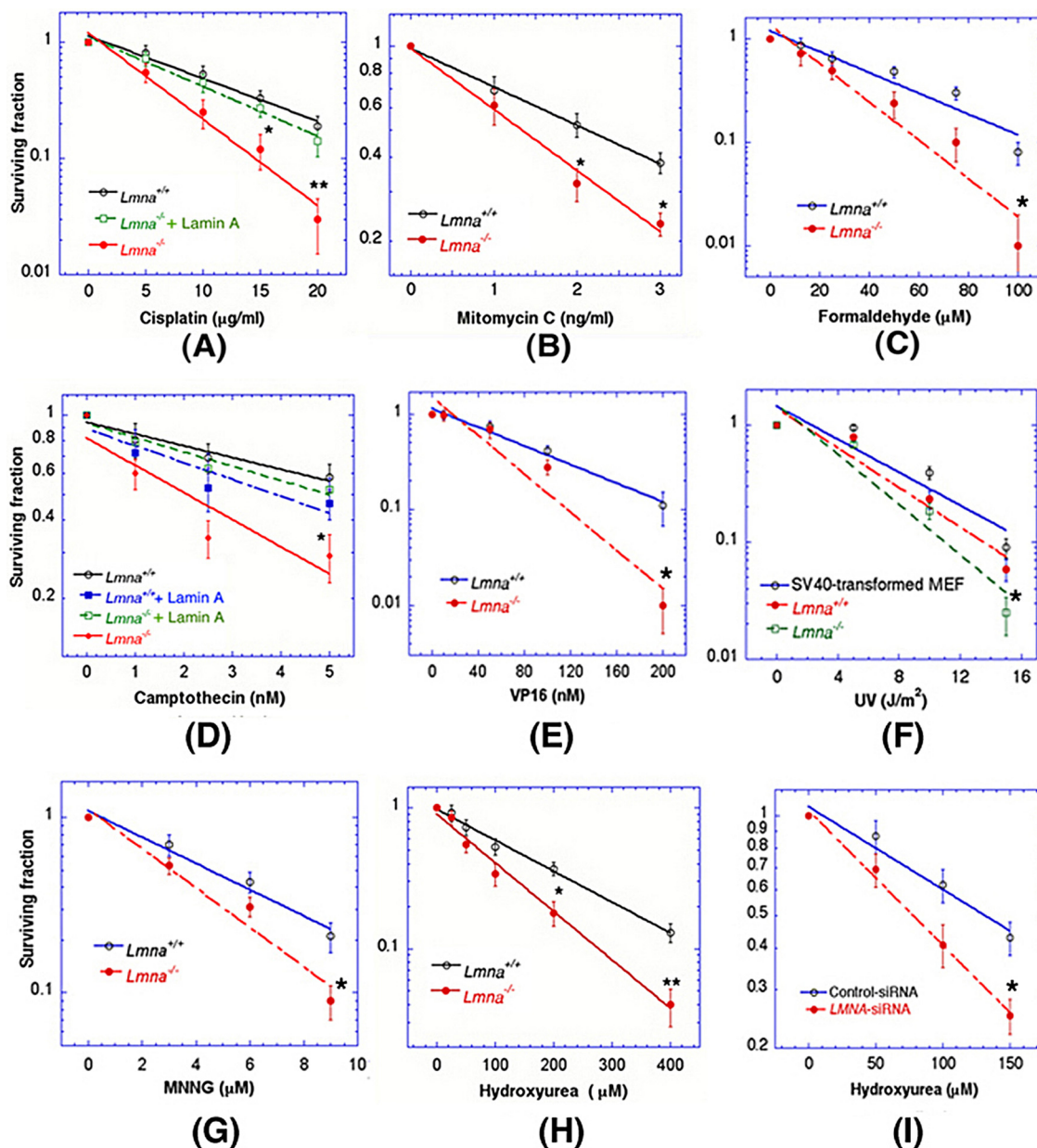


FIG 3 Clonogenic survival of *Lmna*^{-/-}, *Lmna*^{+/+}, and lamin A/C-depleted 293 cells treated with DNA-damaging agents. For survival assay, the required number of cells were plated, incubated for 6 h, treated with the indicated doses of drug or irradiated with UV, and incubated for 10 to 12 days to form countable colonies. *Lmna*^{+/+} cells, *Lmna*^{-/-} cells, and *Lmna*^{-/-} cells with ectopic lamin A expression were treated with cisplatin (A), mitomycin C (B), camptothecin (C), hydroxyurea (D), formaldehyde (F), VP16 (G), UV (H), and MNNG (I). (E) Surviving fraction of 293 cells with and without lamin A/C depletion with specific siRNA after HU treatment. *, *P* < 0.05; **, *P* < 0.01.

are those for transferrin (TF), TRIM25, insulin-like growth factor binding protein 3 (IGFBP3), bone morphogenetic protein 4 (BMP4), and paired-like homeodomain 2 (PITX2). Downregulated genes are those for interleukin 7 (IL-7), interferon regulatory factor 7 (IRF7), lymphocyte antigen 6 complex, locus C1 (LY6C1), FGF7, and LMNA.

Cell death-related genes. Upregulated cell death-related genes are those for PTGIS, TF, KRT8, IGFBP3, and IGFBP6. Downregulated genes are those for matrix Gla protein (MGP), ubiquitin specific peptidase 18 (USP18), necdin homolog (mouse) (NDN), DKK3, and FGF7.

Signal ligand and NF- κ B genes. Upregulated signal ligand and NF- κ B genes are those for IGFBP3, insulin-like growth factor 1 (somatomedin C) (IGF1), intercellular adhesion molecule 1 (ICAM1), vascular endothelial growth factor C (VEGFC), and nuclear factor of kappa light polypeptide gene enhancer in B cells 2 (p49/p100) (NFKB2). Downregulated genes are those for myosin light chain 6B, alkali, smooth muscle and nonmuscle (MYL6B); fibroblast growth factor receptor 1 (FGFR1); signal transducer and activator of transcription 1 (STAT1); IGFBP5; and chemokine (C-C motif) ligand 5 (CCL5).

Lipid metabolism genes. Upregulated lipid metabolism genes

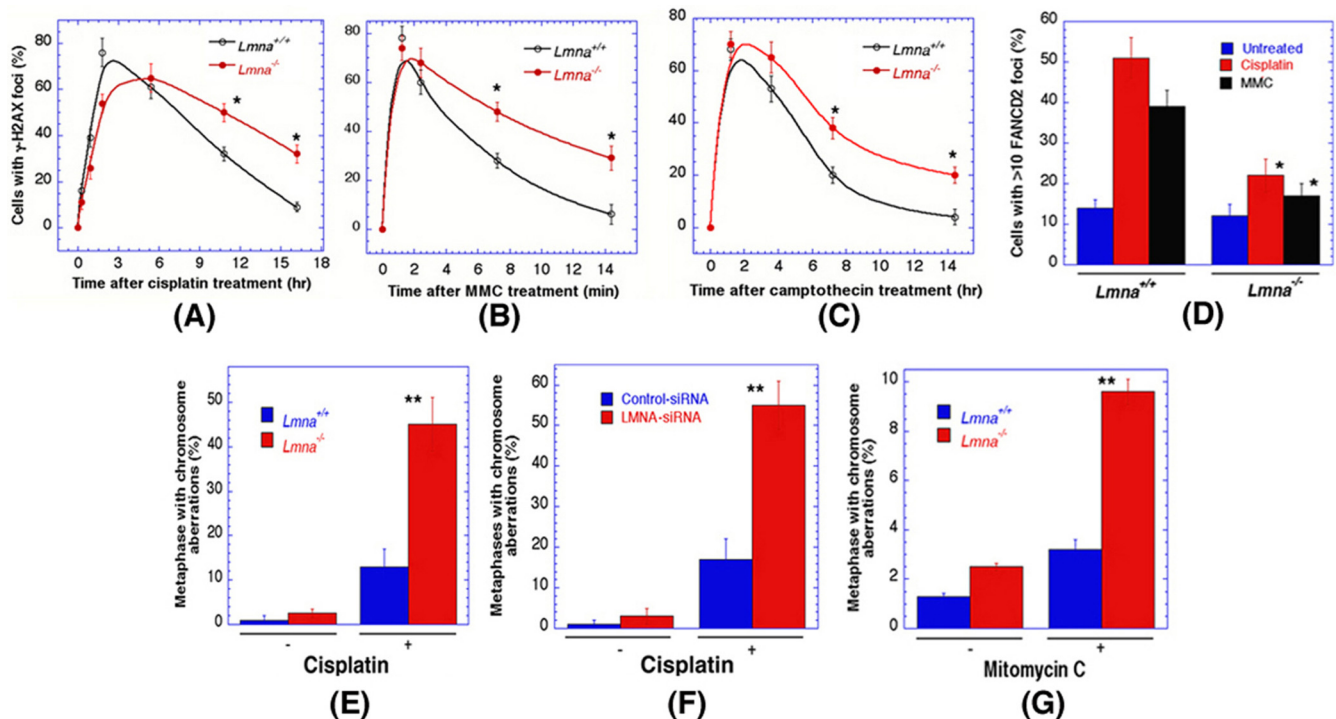


FIG 4 Impaired DNA damage response in lamin A/C-depleted cells. (A to C) Cells with γ -H2AX foci after treatment with cisplatin (A), MMC (B), and camptothecin (C). (D) Cells with FANCD2 foci after cisplatin and MMC treatment. (E) Frequency of *Lmna*^{+/+} and *Lmna*^{-/-} metaphases with chromosome aberrations after cisplatin treatment. (F) Frequency of 293 metaphases with and without lamin A/C with chromosome aberrations after cisplatin treatment. (G) Frequency of *Lmna*^{+/+} and *Lmna*^{-/-} metaphases with chromosome aberrations after MMC treatment. *, $P < 0.05$; **, $P < 0.01$.

are those for glutathione *S*-transferase alpha 3 (GSTA3), glutathione peroxidase 7 (GPX7), paternally expressed 3 (PEG3), COP9 constitutive photomorphogenic homolog subunit 8 (*Arabidopsis*) (COPS8), and glutathione *S*-transferase kappa 1 (GSTK1). Downregulated genes those for are corneodesmosin (CDSN), microsomal glutathione *S*-transferase 3 (MGST3), adrenomedullin (ADM), glutathione *S*-transferase alpha 5 (GSTA5), and LMNA.

Glutathione metabolism genes. Upregulated glutathione metabolism genes are those for GSTA3, GPX7, GSTK1, GSTA4, and MGST1. Downregulated genes are those for acyl coenzyme A synthetase short-chain family member 2 (ACSS2), glutathione *S*-transferase theta 3 (GSTT3), glutaredoxin (thioltransferase) (GLRX), MGST3, and GSTA5.

Interferon signaling genes. The upregulated interferon signaling gene is that for Janus kinase 2 (JAK2) (only one gene is upregulated in this category). Downregulated genes are those for STAT2; transporter 1, ATP-binding cassette, subfamily B (MDR/TAP) (TAP1); myxovirus (influenza virus) resistance 1, interferon-inducible protein p78 (mouse) (MX1); 2',5'-oligoadenylate synthetase 1 (OAS1); and IFIT3.

Ubiquitin pathway genes. *Lmna*^{-/-} cells have 230-fold decreased USP18 levels compared to those of *Lmna*^{+/+} cells.

Specifically, cyclin D1 mRNA was significantly downregulated in *Lmna*^{-/-} cells (Fig. 1C), and consequently cyclin D1 protein was barely detectable in *Lmna*^{-/-} cells (Fig. 1D). Ectopic lamin A expression in *Lmna*^{-/-} cells restored cyclin D1 to the levels observed in *Lmna*^{+/+} cells (Fig. 1D). Similarly, in human 293 cells, siRNA depletion of lamin A/C (Fig. 1E) greatly reduced cyclin D1 levels (Fig. 1F). In addition, cyclin D1 coimmunoprecipitates with

lamin A, suggesting the two proteins interact either directly or indirectly (Fig. 1G).

Role of lamin A/C on ionizing radiation response. Jirawatnotai et al. (37) reported that cyclin D1 plays a role in ionizing radiation response and DNA repair, and we observed that exponentially growing *Lmna*^{-/-} MEFs and human 293 cells depleted for lamin A/C had marginally higher survival postirradiation than the respective control cells (Fig. 2A and data not shown); however, the differences were not statistically significant. This was unexpected, since lamin A/C-deficient cells have reduced levels of cyclin D1 (Fig. 1D and F). Cyclin D1 interacts with DNA repair proteins, and cyclin D1 depletion was previously shown to reduce postirradiation survival (37). Depletion of cyclin D1 from *Lmna*^{+/+} cells (Fig. 2B) did, however, reduce clonogenic survival postirradiation (Fig. 2C), in line with the previously published results, suggesting that lamin A/C depletion reverses the increase in ionizing radiation (IR)-induced cell death resulting from cyclin D1 depletion.

Consistent with the clonogenic survival results, comparison of *Lmna*^{-/-} to *Lmna*^{+/+} exponential-phase cells following IR exposure did not reveal any significant difference in the DDR as determined by the appearance/disappearance kinetics of γ -H2AX foci (Fig. 2D). Similarly, 53BP1, Rad51, FANCD2, CtIP, and RAP80 focus formation in exponential-phase *Lmna*^{-/-} or *Lmna*^{+/+} cells was nearly identical (Fig. 2E and F and data not shown). In addition, neither ATM nor DNA-dependent protein kinase (DNA-PK) phosphorylation following irradiation was altered by lamin A/C loss (Fig. 2G and H). Furthermore, when cells were irradiated in different phases of the cell cycle, the frequency of residual chromosome aberrations observed at metaphase was similar in

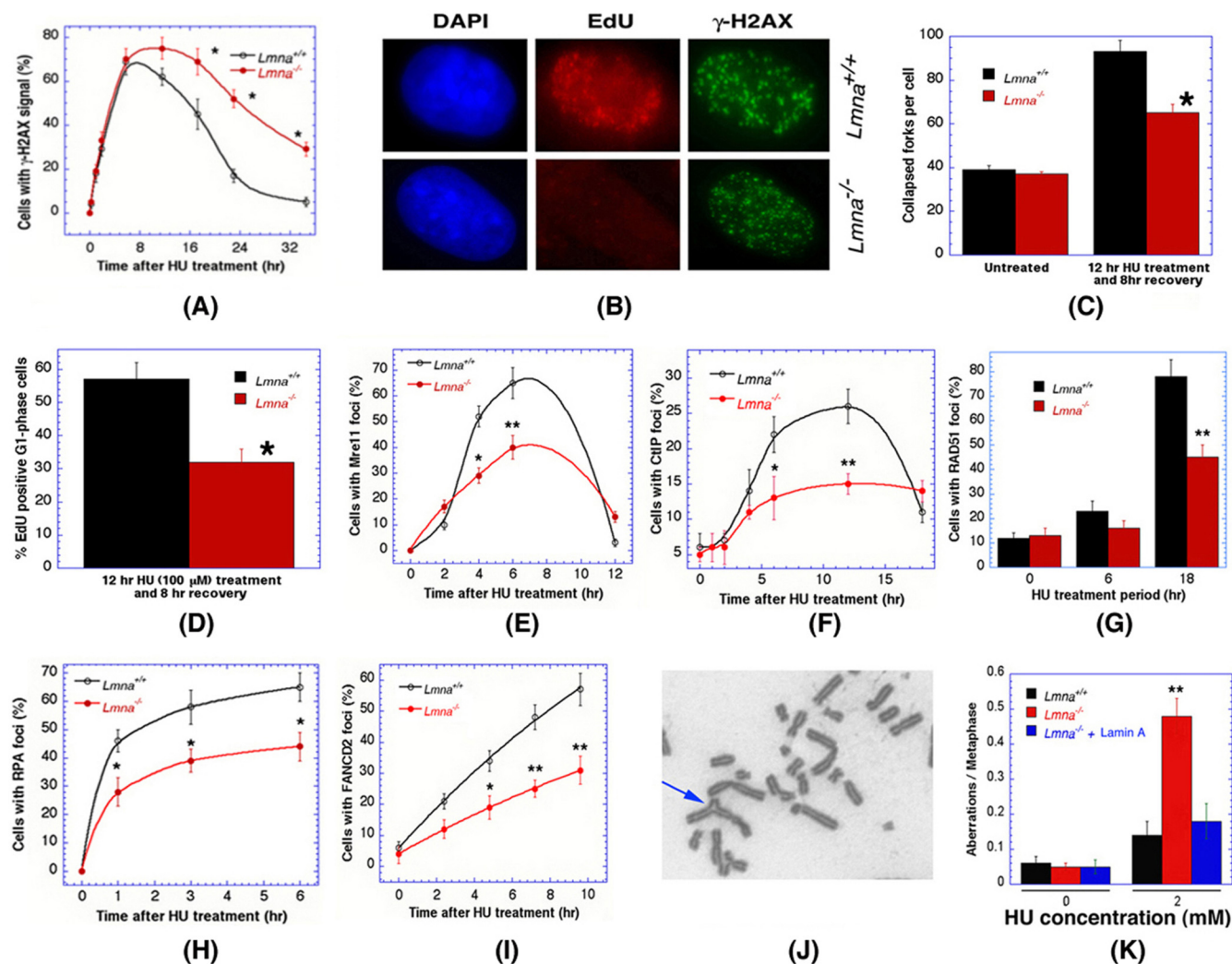


FIG 5 Hydroxyurea treatment response in cells with and without lamin A/C. (A) Frequency of cells with γ -H2AX at different time points after treatment. (B) $Lmna^{+/+}$ and $Lmna^{-/-}$ cells stained for DNA with DAPI and γ -H2AX immunostaining. EdU-positive S/G₂ cells (selected by DAPI staining) were selected only for γ -H2AX focus counting. (C) The number of larger γ -H2AX foci counted in late S/G₂-phase cells in $Lmna^{+/+}$ and $Lmna^{-/-}$ cells represent collapsed forks. The quantification of EdU-positive late S/G₂-phase cells was performed by using scatter blots obtained by scanning the slides for DAPI and EdU intensity. γ -H2AX foci were counted in ~40 cells per data point and experiment per slide. (D) Histogram showing percent EdU-positive G₁ cells. A total of 3,000 cells were counted, and the means from three experiments are plotted. *, $P < 0.05$; **, $P < 0.01$. (E to H) Frequency of cells with Mre11 (E), CtIP foci (F), RAD51 (G), RPA (H), and FANCD2 (I) foci after HU treatment. (J) HU-treated lamin A/C-depleted 293 cells at metaphase with chromosome aberrations, including a triradial (arrow). (K) Histogram showing a comparison of chromosome aberrations per metaphase in $Lmna^{-/-}$ cells, $Lmna^{+/+}$ cells, and $Lmna^{-/-}$ cells with ectopic expression of lamin A.

$Lmna^{-/-}$ and $Lmna^{+/+}$ cells (Fig. 2I). Lamin A/C therefore appears to play no role in the cellular response to ionizing radiation as determined by clonogenic cell survival, DNA damage signaling, or chromosome repair.

Response of lamin A/C-deficient cells to DNA cross-linking and adduct-inducing agents. The results described above indicate that IR-induced DDR in lamin A/C-deficient cells is largely unaltered. Therefore, we asked whether lamin A/C is involved in the repair of DNA intra- or interstrand cross-links (ICLs) or simple DNA adduct damage. ICLs create obstructions to fundamental DNA transactions and are repaired predominantly during S-phase, initiated by replication fork convergence at ICL sites (38). As measured by cell survival, $Lmna^{-/-}$ cells were more sensitive to intra- and interstrand cross-linking agents like cisplatin,

mitomycin C (MMC), and formaldehyde (Fig. 3A, B, and C). The $Lmna^{-/-}$ cells were more sensitive to DNA topoisomerase inhibitors like camptothecin and VP16 (Fig. 3D and E) and thymidine dimer formation induced by UV (Fig. 3F). DNA monoalkylating drugs like *N*-methyl-*N'*-nitro-*N*-nitrosoguanidine (MNNG) (Fig. 3G) were also more lethal to $Lmna^{-/-}$ cells. In addition, we found that $Lmna^{-/-}$ cells were much more sensitive to replication stress induced by HU treatment than $Lmna^{+/+}$ cells, as determined by clonogenic assay (Fig. 3H and I). Depletion of lamin A/C from human 293 cells (Fig. 1F) also resulted in hypersensitivity for cell survival to HU (Fig. 3I), and these cells also had a higher frequency of cells with delayed disappearance of γ -H2AX foci/signal after treatment with cisplatin, MMC, camptothecin, or HU compared to cells expressing lamin A/C (Fig. 4A to C and 5A).

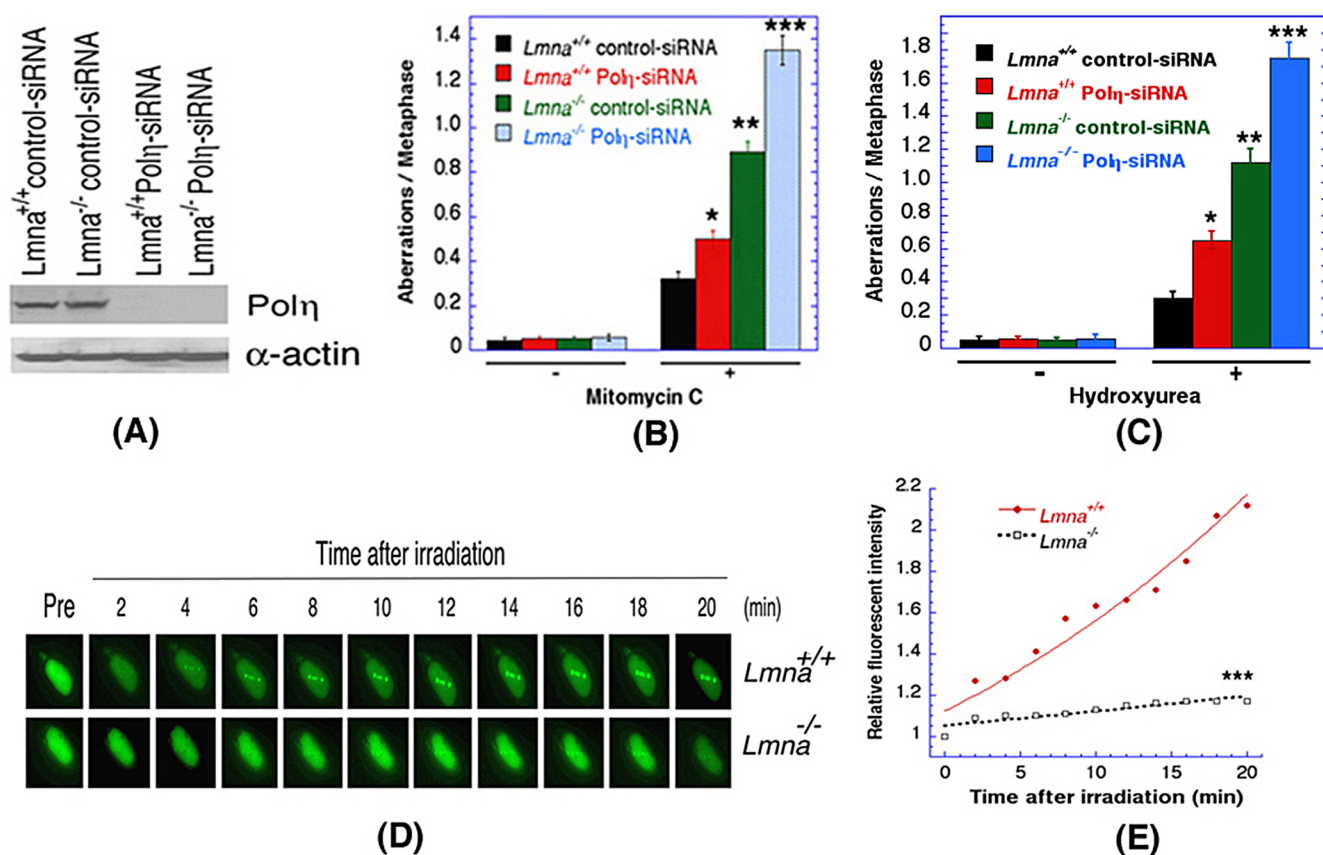


FIG 6 Effect of polymerase η depletion in cells with and without lamin A/C for DNA damage response. (A) Western blot showing polymerase η depletion with specific siRNA in *Lmna*^{+/+} and *Lmna*^{-/-} cells. (B and C) Comparison of chromosome aberrations per metaphase in *Lmna*^{+/+} and *Lmna*^{-/-} cells with and without polymerase η depletion after mitomycin (B) and HU (C) treatment. (D) Recruitment of polymerase η onto laser-induced DNA damage. Exponentially growing *Lmna*^{+/+} and *Lmna*^{-/-} cells transfected with cDNA coding for YFP-polymerase η were microirradiated, and time-lapse images were captured. (E) YFP-polymerase η relative fluorescent intensity kinetics measured in *Lmna*^{+/+} and *Lmna*^{-/-} cells after microirradiation. *, $P < 0.05$; **, $P < 0.01$; ***, $P < 0.005$.

Furthermore, FANCD2 focus induction after cisplatin or MMC treatment was strongly reduced in *Lmna*^{-/-} cells compared to that in *Lmna*^{+/+} cells (Fig. 4D). Both mouse (Fig. 4E) and human (Fig. 4F) lamin A/C-deficient cells displayed a higher frequency of metaphases with chromosome aberrations after cisplatin, mitomycin, or camptothecin treatment compared to cells with lamin A/C (Fig. 4E to G and data not shown). Treatment of *Lmna*^{-/-} cells with HU also significantly delayed the disappearance of γ -H2AX foci (Fig. 5A); reduced the number of large γ -H2AX foci (Fig. 5B), which are an indication of collapsed forks (Fig. 5C); and delayed cell cycle progression (Fig. 5D). Consistent with the observation of abnormally sized γ -H2AX foci, a significant defect in the recruitment of Mre11, CtIP, RAD51, RPA, and FANCD2 into foci was observed in lamin A/C-deficient cells (Fig. 5E to I). In addition, lamin A/C-deficient cells had a high frequency of HU-induced chromosome aberrations, including triradials that could be suppressed by lamin A cDNA expression in *Lmna*^{-/-} cells (Fig. 5J and K).

During repair of DNA strand cross-links, DNA polymerase η plays an important role in translesion DNA synthesis (39, 40). Cells deficient for either lamin A/C or polymerase η (Fig. 6A) had a higher frequency of MMC- and HU-induced chromosome aberrations than cells expressing lamin A/C, and an even higher level of aberrations was observed in doubly deficient cells (Fig. 6B and

C). Furthermore, polymerase η recruitment to UV550-induced DNA damage sites was significantly delayed in *Lmna*^{-/-} cells (Fig. 6D and E). Thus, lamin A/C-deficient cells have compromised DNA interstrand cross-link repair.

Role of lamin A/C in the restart of stalled replication forks.

To determine the mechanism by which lamin A/C deficiency results in defective ICL repair, we compared the restart of stalled replication forks in *Lmna*^{-/-} and *Lmna*^{+/+} cells by using the DNA fiber technique (41). We first determined the frequency of stalled replication forks and new origins. Cells were pulse-labeled with 5-iododeoxyuridine (IdU), treated with HU for different time periods to deplete the nucleotide pool, and then washed and pulse-labeled with 5-chlorodeoxyuridine (CldU) (Fig. 7A) as described previously (42, 43). Replication fork restart was quantified by determining the total number of replication tracks labeled with CldU (Fig. 7B). After removal of the HU block, contiguous IdU/CldU signal, indicating restarting forks, was rarely seen in *Lmna*^{-/-} cells compared to *Lmna*^{+/+} cells that readily resumed DNA synthesis (Fig. 7B to D). Thus, replication had not restarted at the stalled replication forks during the period analyzed in *Lmna*^{-/-} cells. While analyzing DNA fibers (Fig. 7Aii), we found that the percentage of stalled forks in *Lmna*^{-/-} cells after 1 or 21 h of HU treatment was higher than that of *Lmna*^{+/+} cells (Fig. 7E and F). Ectopic expression of lamin A reduced stalled forks and

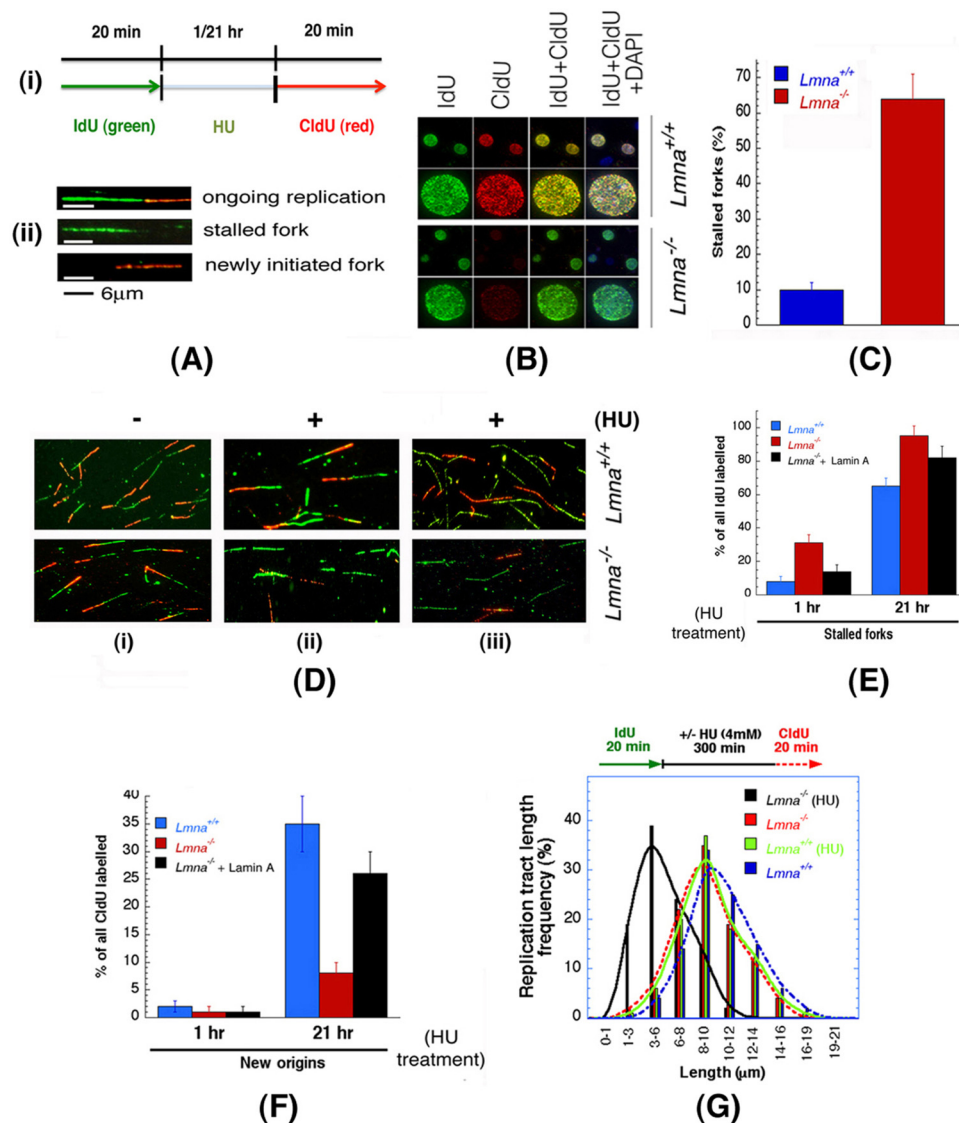


FIG 7 Reinitiation of stalled DNA replication forks and initiation of new origins in *Lmna*^{+/+} and *Lmna*^{-/-} cells. (A) Shown are DNA labeling and HU treatment protocol for single DNA fiber analysis (i) and three major types of labeled DNA tracts for analysis (ii). (B) Comparison of global DNA replication restart after release from 2 h of HU treatment. Cells were prelabeled with IdU, treated with HU, and then postlabeled with CldU, fixed, immunostained with IdU (green) and CldU (red) antibodies, and counterstained with DAPI (blue). Equal intensities of CldU and IdU as well as strong colocalization was observed in *Lmna*^{+/+} MEFs, indicating that DNA replication was able to restart. In contrast, CldU staining in *Lmna*^{-/-} cells was very weak, and little colocalization was detected. (C) Quantification of percentages of cells with stalled forks after HU treatment. *Lmna*^{-/-} cells have the least incorporation of CldU and thus the maximum frequency of cells with stalled forks. (D) Representative images of replication tracks from *Lmna*^{+/+} and *Lmna*^{-/-} cells after 1 h of HU treatment (i), after 21 h of HU treatment (ii), and in cyclin D1-depleted cells after 21 h of HU treatment (iii). (E) Quantification of stalled forks determined by fiber analysis with only IdU signal after 1 or 21 h of HU treatment. *Lmna*^{-/-} cells ectopically expressing lamin A were designated *Lmna*^{-/-} + lamin A. (F) Quantification of new origins as determined by CldU signal after 1 or 21 h of HU treatment. (G) Distribution of IdU track length from DNA fibers from control *Lmna*^{+/+} and *Lmna*^{-/-} cells and *Lmna*^{+/+} and *Lmna*^{-/-} cells treated with HU for 5 h.

increased new origins in *Lmna*^{-/-} cells treated with HU (Fig. 7E and F). To test whether the failure to initiate new replication restart was due to differences in the median IdU track length between *Lmna*^{+/+} and *Lmna*^{-/-} cells, we measured IdU track length with and without treatment of HU for 5 h and found that in HU-treated *Lmna*^{+/+} cells the IdU tract length is maintained, whereas in *Lmna*^{-/-} cells IdU tract length is significantly reduced (Fig. 7G).

Cells deficient in lamin A/C have undetectable levels of cyclin D1 (Fig. 1D and F), which is associated with lamin A in wild-type

cells, but treatment of *Lmna*^{+/+} cells with HU decreases this interaction (Fig. 8A and B). To determine whether the enhanced replication fork stalling seen in *Lmna*^{-/-} cells could be due to low levels of cyclin D1, we examined HU-treated *Lmna*^{-/-} cells with and without ectopic expression of cyclin D1 for stalled forks as well as new origins. Depletion of cyclin D1 significantly increased the number of stalled forks and decreased new origins in *Lmna*^{+/+} but not in *Lmna*^{-/-} cells (Fig. 8C and D). Increased cyclin D1 in *Lmna*^{-/-} cells did not rescue the defect in stalled forks or new origins (Fig. 8E and F). These results

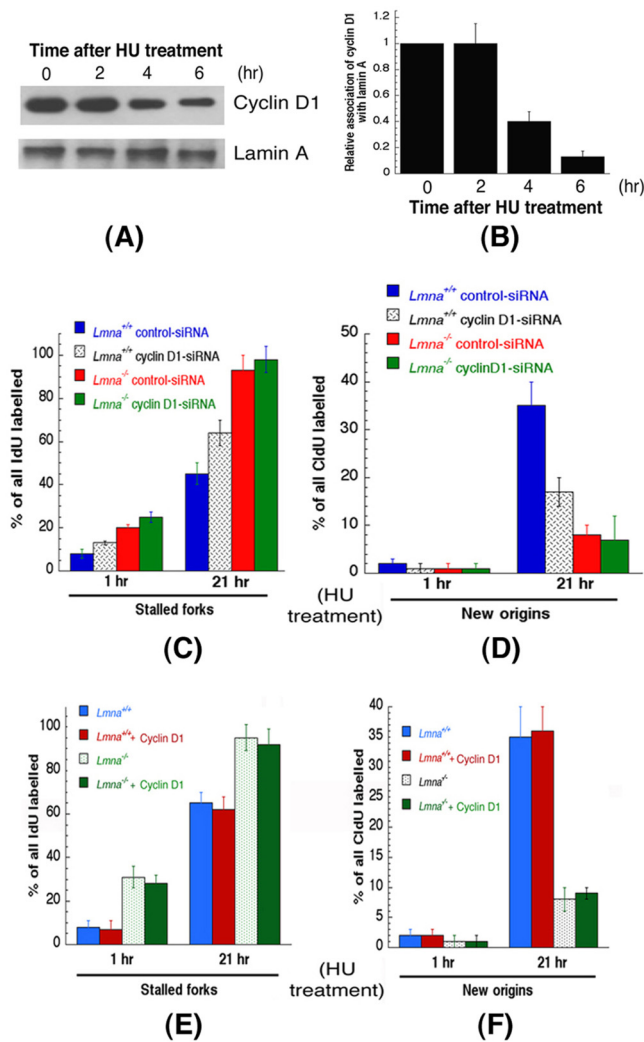


FIG 8 Cyclin D1 is released from lamin A complexes after HU treatment. Cells were treated with 6 mM HU and collected at the indicated times. (A) Lamin A immunoprecipitates blotted for lamin A and cyclin D1. (B) Quantitation of cyclin D1 coimmunoprecipitated by lamin A antibody. The means and SD are from four independent experiments. (C) Effect of cyclin D1 depletion in *Lmna*^{+/+} and *Lmna*^{-/-} cells on stalled forks after 1 or 21 h of HU treatment. (D) Effect of cyclin D1 depletion in *Lmna*^{+/+} and *Lmna*^{-/-} cells on new origins by determining the CldU signal after 1 or 21 h of HU treatment. (E) Frequency of stalled forks in HU-treated *Lmna*^{+/+} and *Lmna*^{-/-} cells with and without ectopic cyclin D1 expression, as determined by DNA fibers analysis of tracks labeled with IdU only. Percentages are based on the total number of IdU tracks that were counted in the different fields. (F) Quantification of new origins in HU-treated *Lmna*^{+/+} and *Lmna*^{-/-} cells, with and without ectopic cyclin D1 expression.

suggest that lamin A has a critical role in the process of stalled replication fork resolution.

Stalled replication fork collapse results in DNA double-strand breaks (DSBs) that are repaired by HR. Since lamin A/C-deficient cells have a high frequency of stalled replication forks, which do not collapse in order to initiate the process of HR for DNA repair, we examined whether DNA DSB repair by HR is different in cells with and without lamin A/C. Since cyclin D1 interacts with Rad51 (37) and cyclin D1 is also associated with lamin A (Fig. 1G), we expected defective HR repair of DNA DSBs in lamin A/C-deficient

cells. However, the frequency of HR repair of a green fluorescent protein (GFP) reporter gene (pDR-GFP) in MCF7 cells after lamin A/C depletion with siRNA (Fig. 9A) was unaltered from the level in control-transfected cells (Fig. 9B), suggesting that lamin A/C does not have a role in DNA DSB repair via the HR pathway.

Lamin A/C is localized to the inner nuclear membrane, and telomeres are known to be associated with the nuclear matrix (44, 46). Telomeres of two sister chromatids at the end of a duplicated chromosome can recombine, and these exchanges are an indication of relaxed control of DNA repair at telomeres. We visualized metaphase chromosomes by chromosome orientation fluorescent *in situ* hybridization (CO-FISH) (26, 36) and measured telomere region recombination events in *Lmna*^{-/-} and *Lmna*^{+/+} cells (Fig. 9C). Neither *Lmna*^{+/+} nor *Lmna*^{-/-} cells displayed any loss of telomere signals or telomere-specific sister chromatid exchanges, indicating that lamin A/C deficiency does not affect telomere stability or global sister chromatid exchange repair processes. Similarly, analysis of *Lmna*^{+/+} and *Lmna*^{-/-} cells for telomere circular DNA (35, 47) did not detect any difference in new arc telomeric DNA (Fig. 9D), indicating a normal recombination phenotype at the telomeres. Thus, the role of lamin A/C in DNA DSB repair is minimal, supporting the argument that lamin A/C plays a critical role in the restart of stalled replication forks (Fig. 9E).

DISCUSSION

LMNA mutations can result in synthesis of altered lamin proteins termed progeria. The accumulation of LMNA mutations may cause chromatin perturbations affecting DDR and DSB production (16). Furthermore, progerin accumulation is proposed to disrupt some replication and repair factor functions. As a result, xeroderma pigmentosum group A protein may mislocate to replication forks and affect replication fork stalling with subsequent DNA DSB induction (16). We compared cells with and without *Lmna* to identify DNA DSB repair-associated genes that are down-regulated in *Lmna*-null cells. The main defect revealed was that *Lmna*-null cells have reduced levels of cyclin D1. Recent studies have shown that reducing cyclin D1 levels in human cancer cells increased sensitivity to IR-induced cell killing, impaired recruitment of RAD51 to damaged DNA, and impeded HR-mediated DNA DSB repair (37). While lamin A/C-deficient cells have decreased cyclin D1 protein levels, they do not display any major IR response defects. Instead, lamin A/C is required for efficient repair of damage induced by agents which cause DNA adducts or lesions that are repaired mostly during S phase. In cultured cells, DNA replication sites can be visualized as discrete early or late replication foci in the nucleoplasm (48), and lamin A/C is present at sites of early replication in normal human fibroblasts (34, 49). The prevalence of triradial chromosomes after treatment with MMC, cisplatin, or HU, as well as the impaired recruitment of DNA polymerase η to UV550 laser-induced damage in *Lmna*^{-/-} cells, strongly suggests defective resolution of stalled replication forks. Replication fork restarts after deoxynucleotide pool depletion indicates how quickly cells are able to recover from a replication block and resume normal DNA synthesis. Lamin A/C-depleted cells were unable to restart most replication forks after treatment with HU compared to cells with lamin A/C, indicating that lamin A/C is required for the resolution of stalled replication forks. DNA fiber analysis confirmed this requirement and indicated that lamin A/C deficiency resulted in shorter track lengths. Since lamin

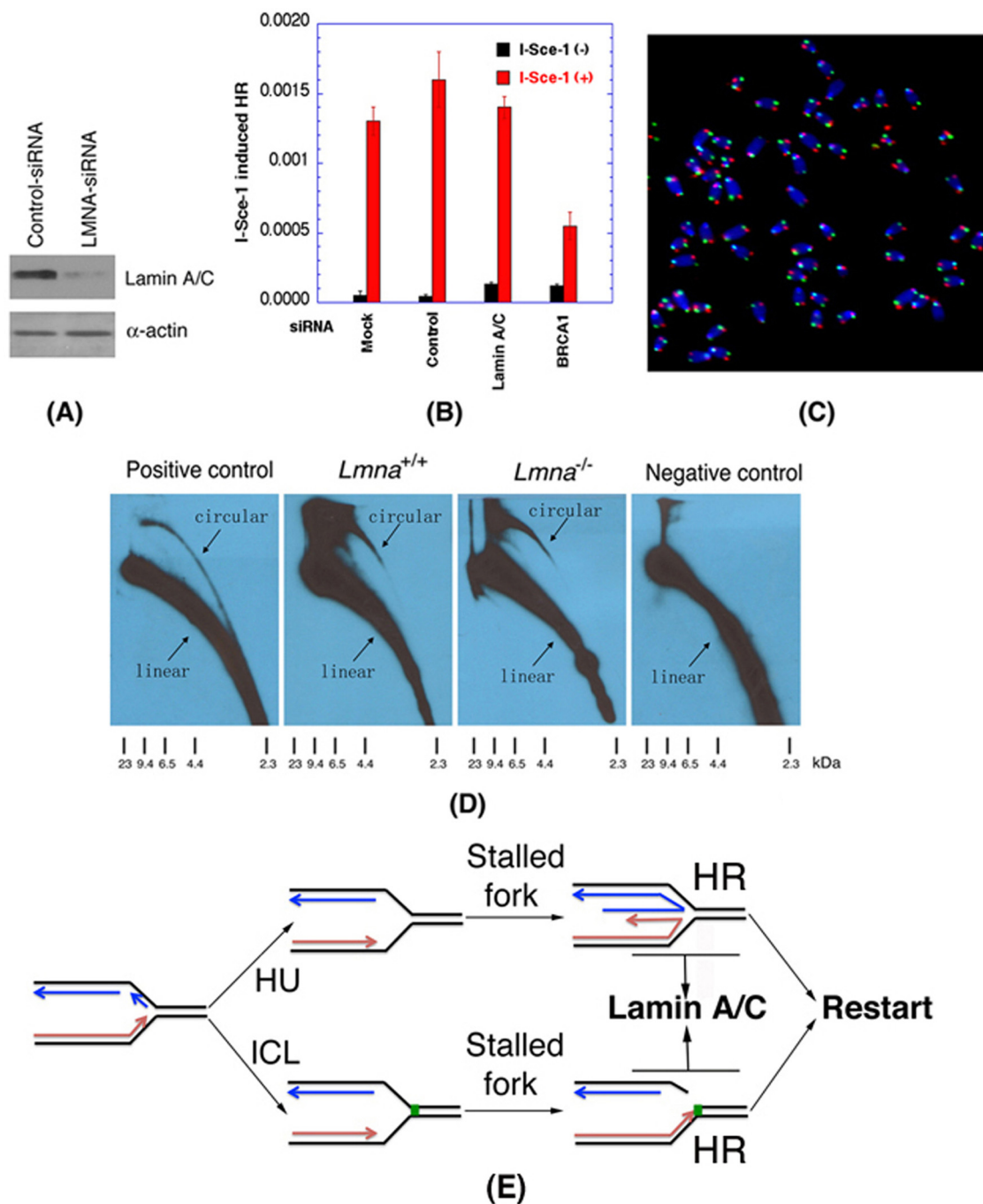


FIG 9 Lamin A/C depletion does not affect DSB repair by homologous recombination. (A) Western blot analysis of lamin A/C depletion in MCF7 cells by siRNA. (B) HR frequencies in MCF7 cells are shown with or without I-Sce-1 induction in untreated cells, in cells treated with control siRNA, and in cells treated with LMNA- or BRCA1-specific siRNA. The results presented are the means and standard errors from three independent experiments. (C) Telomere strand-specific orientation analysis at metaphase. Metaphase chromosome CO-FISH showing strand-specific telomeres was performed as described in Materials and Methods. (D) *Lmna*^{+/+} and *Lmna*^{-/-} cells do not show any difference in telomeric circles. Genomic DNA from *Lmna*^{+/+} and *Lmna*^{-/-} cells was separated by neutral-neutral 2D gel electrophoresis first in size (x axis) and then in shape (y axis), blotted, and probed for telomeric DNA. U2OS cells (ALT cells) were used as a positive control. (E) Model for the role of lamin A/C showing the start of homologous recombination (HR) repair at the proposed site for the collapse of stalled DNA replication forks in order to enable origins to restart and initiate homology-mediated repair.

A/C-deficient cells have normal homology-directed repair as well as repair of IR-induced DNA damage, even in the absence of cyclin D1, such repair may be mechanistically different from ICL and stalled fork repair.

Based on these observations, we speculate that lamin A/C provides a platform for the resolution of stalled replication fork intermediates (Fig. 9E). The platform requires both lamin A/C and cyclin D1. Since cyclin D1 is released from lamin A after HU treat-

ment, release of cyclin D1 from lamin A may be regulating an activity, possibly a nucleolytic step, required for collapse of stalled replication forks prior to initiation of homology-directed repair. Moreover, cyclin D1 interacts with Rad51, which may assist repairosome formation. This is consistent with defective Rad51 focus formation, as well as other repairosome factors related to resection, after HU or cisplatin treatment in *Lmna*^{-/-} cells or cells depleted of cyclin D1. These and other results suggest that the absence of lamin A/C and cyclin D1 impacts the resolution of the stalled replication fork. Based on our results, we propose that lamin A/C provides a platform (Fig. 9E) with a protective function during replication fork stalling that is dependent upon cyclin D1 which in turn interacts with Rad51, thus assisting repairosome formation in a manner that is mechanistically followed by initiation of the HR repair pathway to repair the collapsed stalled forks.

ACKNOWLEDGMENTS

This work was supported by National Institutes of Health/National Cancer Institute grants R01CA129537, R01CA154320, U19A1091175, and R13CA130756 (T.K.P.) and NASA grant NNX11AC15G (J.W.S.).

We acknowledge the assistance of the Genomics Shared Resource at the Harold C. Simmons Cancer Center, which is supported in part by NCI Cancer Center Support Grant 1P30 CA142543. We thank C. L. Stewart for providing reagents, R. Baer for providing CtIP antibody, and S. Mitra and D. Cortez for their helpful suggestions.

M.S., R.K.P., R.K., and T.K.P. designed research; C.-R.Y. performed DNA microarray and IPA network analyses; M.S., C.R.H., R.K.P., R.K., N.H., R.B., S.S., M.D.S., A.G., J.J., S.P., B.P.C.C., D.D., M.L., Q.Y., and T.K.P. performed experiments, provided reagents, and analyzed data; and M.S., C.R.H., J.W.S., S.N.P., K.K.K., H.J.W., and T.K.P. reviewed data analyses and wrote the paper.

REFERENCES

- Lammerding J, Fong LG, Ji JY, Reue K, Stewart CL, Young SG, Lee RT. 2006. Lamins A and C but not lamin B1 regulate nuclear mechanics. *J. Biol. Chem.* 281:25768–25780.
- Goldberg M, Harel A, Brandeis M, Rechsteiner T, Richmond TJ, Weiss AM, Gruenbaum Y. 1999. The tail domain of lamin Dm0 binds histones H2A and H2B. *Proc. Natl. Acad. Sci. U. S. A.* 96:2852–2857.
- Schirmer EC. 2008. The epigenetics of nuclear envelope organization and disease. *Mutat. Res.* 647:112–121.
- Dechat T, Pfliegerhaer K, Sengupta K, Shimi T, Shumaker DK, Solimando L, Goldman RD. 2008. Nuclear lamins: major factors in the structural organization and function of the nucleus and chromatin. *Genes Dev.* 22: 832–853.
- Navarro CL, De Sandre-Giovannoli A, Bernard R, Boccaccio I, Boyer A, Genevieve D, Hadj-Rabia S, Gaudy-Marqueste C, Smitt HS, Vabres P, Faivre L, Verloes A, Van Essen T, Flori E, Hennekam R, Beemer FA, Laurent N, Le Merrer M, Cau P, Levy N. 2004. Lamin A and ZMPSTE24 (FACE-1) defects cause nuclear disorganization and identify restrictive dermopathy as a lethal neonatal laminopathy. *Hum. Mol. Genet.* 13:2493–2503.
- Zhang H, Kieckhafer JE, Cao K. 2012. Mouse models of laminopathies. *Aging Cell* [Epub ahead of print.] doi:10.1111/accel.12021.
- Broers JL, Ramaekers FC, Bonne G, Yaou RB, Hutchinson CJ. 2006. Nuclear lamins: laminopathies and their role in premature ageing. *Physiol. Rev.* 86:967–1008.
- Lees-Miller SP. 2006. Dysfunction of lamin A triggers a DNA damage response and cellular senescence. *DNA Repair (Amsterdam)* 5:286–289.
- Burke B, Stewart CL. 2002. Life at the edge: the nuclear envelope and human disease. *Nat. Rev. Mol. Cell Biol.* 3:575–585.
- Gruenbaum Y, Margalit A, Goldman RD, Shumaker DK, Wilson KL. 2005. The nuclear lamina comes of age. *Nat. Rev. Mol. Cell Biol.* 6:21–31.
- Taddei A, Hediger F, Neumann FR, Gasser SM. 2004. The function of nuclear architecture: a genetic approach. *Annu. Rev. Genet.* 38:305–345.
- Dechat T, Adam SA, Goldman RD. 2009. Nuclear lamins and chromatin: when structure meets function. *Adv. Enzyme Regul.* 49:157–166.
- Sullivan T, Escalante-Alcalde D, Bhatt H, Anver M, Bhat N, Nagashima K, Stewart CL, Burke B. 1999. Loss of A-type lamin expression compromises nuclear envelope integrity leading to muscular dystrophy. *J. Cell Biol.* 147:913–920.
- Puckelwartz MJ, Depreux FF, McNally EM. 2011. Gene expression, chromosome position and lamin A/C mutations. *Nucleus* 2:162–167.
- Shimi T, Pfliegerhaer K, Kojima S, Pack CG, Solovei I, Goldman AE, Adam SA, Shumaker DK, Kinjo M, Cremer T, Goldman RD. 2008. The A- and B-type nuclear lamin networks: microdomains involved in chromatin organization and transcription. *Genes Dev.* 22:3409–3421.
- Musich PR, Zou Y. 2011. DNA-damage accumulation and replicative arrest in Hutchinson-Gilford progeria syndrome. *Biochem. Soc. Trans.* 39:1764–1769.
- Gupta A, Sharma GG, Young CS, Agarwal M, Smith ER, Paull TT, Lucchesi JC, Khanna KK, Ludwig T, Pandita TK. 2005. Involvement of human MOF in ATM function. *Mol. Cell. Biol.* 25:5292–5305.
- Sharma GG, So S, Gupta A, Kumar R, Cayrou C, Avvakumov N, Bhadra U, Pandita RK, Porteus MH, Chen DJ, Cote J, Pandita TK. 2010. MOF and histone H4 acetylation at lysine 16 are critical for DNA damage response and double-strand break repair. *Mol. Cell. Biol.* 30:3582–3595.
- Gupta A, Guerin-Peyrou TG, Sharma GG, Park C, Agarwal M, Ganju RK, Pandita S, Choi K, Sukumar S, Pandita RK, Ludwig T, Pandita TK. 2008. The mammalian ortholog of Drosophila MOF that acetylates histone H4 lysine 16 is essential for embryogenesis and oncogenesis. *Mol. Cell. Biol.* 28:397–409.
- Pandita TK. 2006. Role of mammalian Rad9 in genomic stability and ionizing radiation response. *Cell Cycle* 5:1289–1291.
- Pandita TK, Hittelman WN. 1992. The contribution of DNA and chromosome repair deficiencies to the radiosensitivity of ataxia-telangiectasia. *Radiat. Res.* 131:214–223.
- Pandita TK, Lieberman HB, Lim DS, Dhar S, Zheng W, Taya Y, Kastan MB. 2000. Ionizing radiation activates the ATM kinase throughout the cell cycle. *Oncogene* 19:1386–1391.
- Agarwal M, Pandita S, Hunt CR, Gupta A, Yue X, Khan S, Pandita RK, Pratt D, Shay JW, Taylor JS, Pandita TK. 2008. Inhibition of telomerase activity enhances hyperthermia-mediated radiosensitization. *Cancer Res.* 68:3370–3378.
- Hunt CR, Pandita RK, Laszlo A, Higashikubo R, Agarwal M, Kitamura T, Gupta A, Rief N, Horikoshi N, Baskaran R, Lee JH, Lobrich M, Paull TT, Roti Roti JL, Pandita TK. 2007. Hyperthermia activates a subset of ataxia-telangiectasia mutated effectors independent of DNA strand breaks and heat shock protein 70 status. *Cancer Res.* 67:3010–3017.
- Pandita TK, Westphal CH, Anger M, Sawant SG, Geard CR, Pandita RK, Scherthan H. 1999. Atm inactivation results in aberrant telomere clustering during meiotic prophase. *Mol. Cell. Biol.* 19:5096–5105.
- Gupta A, Yang Q, Pandita RK, Hunt CR, Xiang T, Misri S, Zeng S, Pagan J, Jeffery J, Puc J, Kumar R, Feng Z, Powell SN, Bhat A, Yaguchi T, Wadhwa R, Kaul SC, Parsons R, Khanna KK, Pandita TK. 2009. Cell cycle checkpoint defects contribute to genomic instability in PTEN deficient cells independent of DNA DSB repair. *Cell Cycle* 8:2198–2210.
- Pandita RK, Sharma GG, Laszlo A, Hopkins KM, Davey S, Chakhp-aronian M, Gupta A, Wellinger RJ, Zhang J, Powell SN, Roti Roti JL, Lieberman HB, Pandita TK. 2006. Mammalian Rad9 plays a role in telomere stability, S- and G2-phase-specific cell survival, and homologous recombinational repair. *Mol. Cell. Biol.* 26:1850–1864.
- Vafa O, Wade M, Kern S, Beeche M, Pandita TK, Hampton GM, Wahl GM. 2002. c-Myc can induce DNA damage, increase reactive oxygen species, and mitigate p53 function: a mechanism for oncogene-induced genetic instability. *Mol. Cell* 9:1031–1044.
- Jackson DA, Pombo A. 1998. Replicon clusters are stable units of chromosome structure: evidence that nuclear organization contributes to the efficient activation and propagation of S phase in human cells. *J. Cell Biol.* 140:1285–1295.
- Petermann E, Helleday T. 2010. Pathways of mammalian replication fork restart. *Nat. Rev. Mol. Cell Biol.* 11:683–687.
- Sharma GG, Gupta A, Wang H, Scherthan H, Dhar S, Gandhi V, Iliakis G, Shay JW, Young CS, Pandita TK. 2003. hTERT associates with human telomeres and enhances genomic stability and DNA repair. *Oncogene* 22:131–146.
- Sharma GG, Hwang KK, Pandita RK, Gupta A, Dhar S, Parenteau J, Agarwal M, Worman HJ, Wellinger RJ, Pandita TK. 2003. Human heterochromatin protein 1 isoforms HP1(Hsalpha) and HP1(Hsbeta) interfere with hTERT-telomere interactions and correlate with changes in

- cell growth and response to ionizing radiation. *Mol. Cell. Biol.* 23:8363–8376.
33. Pandita TK, Pathak S, Geard CR. 1995. Chromosome end associations, telomeres and telomerase activity in ataxia telangiectasia cells. *Cytogenet. Cell Genet.* 71:86–93.
 34. Kennedy BK, Barbie DA, Classon M, Dyson N, Harlow E. 2000. Nuclear organization of DNA replication in primary mammalian cells. *Genes Dev.* 14:2855–2868.
 35. Cohen S, Lavi S. 1996. Induction of circles of heterogeneous sizes in carcinogen-treated cells: two-dimensional gel analysis of circular DNA molecules. *Mol. Cell. Biol.* 16:2002–2014.
 36. Pandita TK, DeRubeis D. 1995. Spontaneous amplification of interstitial telomeric bands in Chinese hamster ovary cells. *Cytogenet. Cell Genet.* 68:95–101.
 37. Jirawatnotai S, Hu Y, Michowski W, Elias JE, Becks L, Bienvenu F, Zagodzón A, Goswami T, Wang YE, Clark AB, Kunkel TA, van Harn T, Xia B, Correll M, Quackenbush J, Livingston DM, Gygi SP, Sicinski P. 2011. A function for cyclin D1 in DNA repair uncovered by protein interactome analyses in human cancers. *Nature* 474:230–234.
 38. Raschle M, Knipscheer P, Enoiu M, Angelov T, Sun J, Griffith JD, Ellenberger TE, Schärer OD, Walter JC. 2008. Mechanism of replication-coupled DNA interstrand crosslink repair. *Cell* 134:969–980.
 39. Biertumpfel C, Zhao Y, Kondo Y, Ramon-Maiques S, Gregory M, Lee JY, Masutani C, Lehmann AR, Hanaoka F, Yang W. 2010. Structure and mechanism of human DNA polymerase ϵ . *Nature* 465:1044–1048.
 40. Silverstein TD, Johnson RE, Jain R, Prakash L, Prakash S, Aggarwal AK. 2010. Structural basis for the suppression of skin cancers by DNA polymerase ϵ . *Nature* 465:1039–1043.
 41. Henry-Mowatt J, Jackson D, Masson JY, Johnson PA, Clements PM, Benson FE, Thompson LH, Takeda S, West SC, Caldecott KW. 2003. XRCC3 and Rad51 modulate replication fork progression on damaged vertebrate chromosomes. *Mol. Cell* 11:1109–1117.
 42. Petermann E, Orta ML, Issaeva N, Schultz N, Helleday T. 2010. Hydroxyurea-stalled replication forks become progressively inactivated and require two different RAD51-mediated pathways for restart and repair. *Mol. Cell* 37:492–502.
 43. Schlacher K, Christ N, Siaud N, Egashira A, Wu H, Jasin M. 2011. Double-strand break repair-independent role for BRCA2 in blocking stalled replication fork degradation by MRE11. *Cell* 145:529–542.
 44. de Lange T. 1992. Human telomeres are attached to the nuclear matrix. *EMBO J.* 11:717–724.
 45. Reference deleted.
 46. Smilenov LB, Dhar S, Pandita TK. 1999. Altered telomere nuclear matrix interactions and nucleosomal periodicity in ataxia telangiectasia cells before and after ionizing radiation treatment. *Mol. Cell. Biol.* 19:6963–6971.
 47. Brewer BJ, Fangman WL. 1987. The localization of replication origins on ARS plasmids in *S. cerevisiae*. *Cell* 51:463–471.
 48. Moir RD, Yoon M, Khuon S, Goldman RD. 2000. Nuclear lamins A and B1: different pathways of assembly during nuclear envelope formation in living cells. *J. Cell Biol.* 151:1155–1168.
 49. Shumaker DK, Solimando L, Sengupta K, Shimi T, Adam SA, Grunwald A, Strelkov SV, Aebi U, Cardoso MC, Goldman RD. 2008. The highly conserved nuclear lamin Ig-fold binds to PCNA: its role in DNA replication. *J. Cell Biol.* 181:269–280.